Numerical simulations of three-dimensional foam by the immersed boundary method

Yongsam Kim*, Ming-Chih Lai†, Charles S. Peskin‡, Yunchang Seol§

Abstract

In this paper, we present an immersed boundary (IB) method to simulate a dry foam, i.e., a foam in which most of the volume is attributed to its gas phase. Dry foam dynamics involves the interaction between a gas and a collection of thin liquid-film internal boundaries that partition the gas into discrete cells or bubbles. The liquid film boundaries are flexible, contract under the influence of surface tension, and are permeable to the gas, which moves across them by diffusion at a rate proportional to the local pressure difference across the boundary. Such problems are conventionally studied by assuming that the pressure is uniform within each bubble. Here, we introduce instead an IB method that takes into account the non-equilibrium fluid mechanics of the gas. To model gas diffusion across the internal liquid-film boundaries, we allow normal slip between the boundary and the gas at a velocity proportional to the (normal) force generated by the boundary surface tension. We implement this method in the three-dimensional case, and test it by verifying the 3D generalization of von-Neumann relation, which governs the coarsening of a three-dimensional dry foam.

*Department of Mathematics, Chung-Ang University, Dongjakgu Heukseokdong, Seoul 156-756, Korea, kimy@cau.ac.kr; 82.2.820.5219 (voice); 82.2.820.5214 (fax)

†Department of Applied Mathematics, Institute of Mathematical Modeling and Scientific Computing, National Chiao Tung University, 1001, Ta Hsueh Road, Hsinchu 300, Taiwan, mclai@math.nctu.edu.tw

‡Courant Institute of Mathematical Sciences, New York University, 251 Mercer Street, New York, NY 10012 USA. peskin@cims.nyu.edu; 212.998.3126 (voice); 212.995.4121 (fax)

§Department of Mathematics, Chung-Ang University, Dongjakgu Heukseokdong, Seoul 156-756, Korea, iceberg99@hanmail.net; 82.2.820.5214 (fax)

Keywords: foam, permeability, capillary-driven motion, von Neumann relation, immersed boundary method

AMS subject classifications: 65-04, 65M06, 76D05, 76M20

1 Introduction

We use an immersed boundary (IB) method to simulate a "dry" foam in 3D, i.e., a foam in which most of the volume is attributed to its gas phase. Liquid foams appear in daily life as the soap froth in a washing bowl or the head on a pint of bear. A foam is a gas-liquid mixture in which the volume of liquid is considerably smaller than that of the gas. One interesting phenomenon, which is called diffusive coarsening, is the evolution in bubble size and topological structure that occurs as a result of gas exchange between bubbles [1]. This gas exchange occurs by diffusion through the thin liquid films that separate one bubble from another. The diffusive flux of gas through such a film is proportional to the pressure difference between the two bubbles that are separated by that film.

In 1952, von Neumann [2, 3] showed that the rate of the change of the area of a given bubble (a curved polygon) in two-dimensional dry foam is independent of bubble size and solely dependent on the number of walls (or edges). The derivation is based on the fact that the net rate of outward diffusion of gas per unit length through a wall of the (two-dimensional) bubble is proportional to the pressure difference across that wall, which in turn is equal to the product of the surface tension γ and the curvature κ. The rate of area change of a bubble reads

$$\frac{dA}{dt} = -M\,\gamma \int_\Gamma \kappa\, dl = -2\pi M\gamma(1 - n/6), \tag{1}$$

where M is a permeability coefficient, the curve Γ is the closed boundary of the bubble, dl is the arc length along Γ, and n is the number of walls. The second equality can be proved by using the fact that the boundary of the bubble is a closed curve and that each of the exterior (turning) angles at the vertex (triple junction) must be equal to $2\pi/6$.

Until very recently, the von Neumann relation generalized to three-dimensional foams has finally been developed in [4, 5]. Similar to 2D von Neumann relation, the net rate of outward diffusion of gas per unit area through a wall of the (three-dimensional) bubble is proportional to $\gamma\, H$ where H is the mean curvature, that is the sum of the two principle curvatures. Let V be the volume of a bubble $\mathbf{D}$, the rate of volume change is

$$\frac{dV}{dt} = -M\,\gamma \int_{\partial \mathbf{D}} H\, dS = -2\pi M\,\gamma\,(\mathcal{L}(\mathbf{D}) - \frac{1}{6}\sum_{i=1}^{n} e_i(\mathbf{D})). \tag{2}$$

Here the quantity $\mathcal{L}(\mathbf{D})$ is a natural measure of the linear size of bubble $\mathbf{D}$, e_i is the length of each triple line (edge), and the summation is over all n triple lines of $\mathbf{D}$. The relation is based on the fact that each of the dihedral angles along edge is equal to $2\pi/6$ and on the ingeniously defined mean width $\mathcal{L}(\mathbf{D})$ which is computed in two steps. First, for each line l through the origin, Euler width $E_l(\mathbf{D})$ is defined as the integral along l of the Euler characteristic $\chi(l_p^{\perp} \cap \mathbf{D})$ of the intersection of $\mathbf{D}$ with the plane perpendicular to l:

$$E_l(\mathbf{D}) = \int_p \chi(l_p^{\perp} \cap \mathbf{D}) dp. \tag{3}$$

Then $\mathcal{L}(\mathbf{D})$ is twice the Euler width, averaged over all lines l through the origin. The supplementary information for [5] gives the proof of the 3D formula (2) and the schemes for computing the mean width $\mathcal{L}(\mathbf{D})$.

In [6], the authors have presented an immersed boundary (IB) method and simulated the fluid dynamics of a two-dimensional dry foam by modeling the gas phase of the foam as a viscous incompressible fluid, and the liquid phase as a massless network of permeable internal boundaries under surface tension. The gas diffusion through the liquid phase of the foam was modeled by allowing the internal boundaries to slip relative the fluid, at a velocity (speed *and* direction) proportional to the boundary force [6, 7]. The paper [6] has shown that the IB method is a proper tool to simulate the 2D foam dynamics by verifying the von-Neumann relation and simulating foams with an arbitrarily general shape.

Here we extend the methodology introduced in [6] and present the IB method to study the three-dimensional dry foam dynamics. Although we basically use the same idea as

in [6], the mathematical derivation and numerical implementation are complicated enough to require the detailed description. Particularly in 3D, the bubble boundaries which are surfaces can be expressed using the triangulation, and the force on the surfaces is dependent on the mean curvature on the vertices of each triangle. Moreover, an algorithm is needed to maintain the resolution of each internal boundary within predetermined bounds despite arbitrarily large changes in area of the internal boundary.

The rest of the paper is organized as follows. In Section 2, we describe the equations of motion of the foam in immersed boundary form. These are the typical IB equations of motion, generalized to handle a permeable boundary under surface tension. The numerical implementation including external boundary conditions is described in Section 3. In Section 4, we present simulation results: first, we validate the method by doing a convergence study and by showing numerically that the 3D generalized von Neumann relation is satisfied. Then we consider more complicated cases: one is the case in which non-equilibrium flows of gas occur within each cell of the foam, thus requiring the full fluid dynamics treatment of the present paper, and the other case is the general foam. Conclusions and future work are discussed in Section 5.

2 Equations of Motion

In this section, we state the equations of motion of a three-dimensional dry foam, in which the boundaries between bubbles are idealized as massless surfaces under a constant surface tension γ. These boundaries are assumed permeable to the gas phase of the foam, with permeability coefficient M. The gas phase is modeled as a viscous incompressible fluid, for reasons that have been stated in the previous section. The constant density and viscosity of the gas are denoted ρ and μ, respectively.

In the following formulation, the parameter (r, s) labels a material point of an internal foam boundary. We assume that distinct points of the parameter (r, s) are used for the different internal foam boundaries, so that any particular value of (r, s) occurs on at most

one internal boundary. An integral with respect to (r, s) with no stated limit of integration should be understood to mean an integral over the union of all of the internal foam boundaries. With this understanding, the equations of motion are as follows.

$$\rho(\frac{\partial \mathbf{u}}{\partial t} + \mathbf{u} \cdot \nabla \mathbf{u}) = -\nabla p + \mu \nabla^2 \mathbf{u} + \mathbf{f}, \tag{4}$$

$$\nabla \cdot \mathbf{u} = 0, \tag{5}$$

$$\mathbf{F}(r, s, t) = -\frac{\partial E}{\partial \mathbf{X}}, \tag{6}$$

$$\mathbf{f}(\mathbf{x}, t) = \int \mathbf{F}(r, s, t) \delta(\mathbf{x} - \mathbf{X}(r, s, t)) dr ds, \tag{7}$$

$$\begin{aligned} \frac{\partial \mathbf{X}}{\partial t}(r, s, t) &= \mathbf{u}(\mathbf{X}(r, s, t), t) + M\, \mathbf{F} / \left| \frac{\partial \mathbf{X}}{\partial r} \times \frac{\partial \mathbf{X}}{\partial s} \right|, \\ &= \int \mathbf{u}(\mathbf{x}, t) \delta(\mathbf{x} - \mathbf{X}(r, s, t)) d\mathbf{x} + M\, \mathbf{F} / \left| \frac{\partial \mathbf{X}}{\partial r} \times \frac{\partial \mathbf{X}}{\partial s} \right|, \end{aligned} \tag{8}$$

Eqs. (4)-(5) are the familiar Navier-Stokes equations for a viscous incompressible fluid. The unknown functions in the fluid equations are the fluid velocity, $\mathbf{u}(\mathbf{x}, t)$; the fluid pressure, $p(\mathbf{x}, t)$; and the force density applied by the immersed boundary to the fluid, $\mathbf{f}(\mathbf{x}, t)$, where $\mathbf{x} = (x, y, z)$ are fixed Cartesian coordinates, and t is the time.

Eq. (6) is the foam boundary equation which is written in Lagrangian form. The unknown $\mathbf{X}(r, s, t)$ completely describes the motion of the foam boundary and also its spatial configuration at any given time. The force density $\mathbf{F} = \mathbf{F}(r, s, t)$ is applied by the immersed boundary to the fluid, in the sense that $\mathbf{F}(r, s, t) dr ds$ is the force applied to the fluid by the patch of immersed boundary $dr ds$. This force density is given by the variational derivative $-\frac{\partial E}{\partial \mathbf{X}}$ of the elastic energy functional $E[\mathbf{X}(\cdot, \cdot, t)]$ of the form

$$E[\mathbf{X}(\cdot, \cdot, t)] = \gamma \int \left| \frac{\partial \mathbf{X}}{\partial r} \times \frac{\partial \mathbf{X}}{\partial s} \right| dr ds, \tag{9}$$

which is simply the constant surface tension γ times the total area of the internal foam boundary. It is important to note that, from Eqs. (6) and (9), the boundary force density $\mathbf{F}$ is normal to the boundary, see the Appendix. The fact that $\mathbf{F}$ is normal to the boundary simplifies the formulation of the problem, as explained in more detail below.

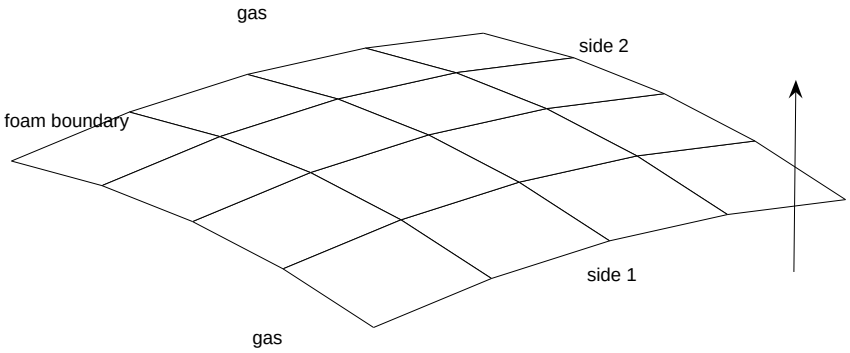

Figure 1: A foam boundary with permeability.

Eqs. (7) and (8) both involve the three-dimensional Dirac delta function $\delta(\mathbf{x}) = \delta(x)\delta(y)\delta(z)$, which express the local character of the interaction between the fluid and boundary. Eq. (7) simply expresses the relation between the two corresponding force densities $\mathbf{f}(\mathbf{x}, t)d\mathbf{x}$ and $\mathbf{F}(r, s, t)drds$. Eq. (8) is the equation of motion of the immersed foam boundary in which M is the permeability constant. In order to derive Eq. (8), we start with the special case of zero permeability. When the permeability $M = 0$, Eq. (8) becomes the familiar no-slip condition. In the following, we use the notation $\mathbf{U}(r, s, t)$ to represent the fluid velocity evaluated at the boundary point $\mathbf{X}(r, s, t)$, i.e,

$$\mathbf{U}(r, s, t) = \mathbf{u}(\mathbf{X}(r, s, t), t) = \int \mathbf{u}(\mathbf{x}, t)\delta(\mathbf{x} - \mathbf{X}(r, s, t))d\mathbf{x}. \tag{10}$$

Now we consider the nonzero permeability of the foam boundary. We assume that the gas (fluid) goes through the liquid-film boundary only in the normal direction. Consider a patch of the boundary of which the area is $\left|\frac{\partial \mathbf{X}}{\partial r} \times \frac{\partial \mathbf{X}}{\partial s}\right| drds$. The net amount of gas per unit time transported through the patch will be proportional to the pressure difference and the area of the patch. This means that the flux through the patch is equal to $M(p_1 - p_2)\left|\frac{\partial \mathbf{X}}{\partial r} \times \frac{\partial \mathbf{X}}{\partial s}\right| drds$ where M is the permeability and p_1 and p_2 are the pressures on the two sides of the foam boundary, see Figure 1. We assume here that the thickness of the foam boundary is a constant. (Otherwise, the flux could also be inversely proportional to the thickness of the foam boundary.)

The flux through the patch can be also evaluated by considering the difference between

the fluid velocity at the internal boundary and the velocity of the boundary itself. That is, the flux can be written as

$$\mathbf{n}(r,s,t)\cdot(\mathbf{U}(r,s,t)-\frac{\partial \mathbf{X}}{\partial t}(r,s,t))\left|\frac{\partial \mathbf{X}}{\partial r}\times\frac{\partial \mathbf{X}}{\partial s}\right|drds. \tag{11}$$

where $\mathbf{n}(r,s,t)$ is the unit normal to the internal boundary. Setting the above two expressions for the flux equal to each other, we get

$$M(p_1-p_2)=\mathbf{n}(r,s,t)\cdot(\mathbf{U}(r,s,t)-\frac{\partial \mathbf{X}}{\partial t}(r,s,t)). \tag{12}$$

From the normal component of mechanical equilibrium at the foam boundary, we see that the pressure jump (p_1-p_2) can be related to the normal component of the boundary force $\mathbf{F}(r,s,t)$ [13, 14] as

$$(p_1-p_2)\left|\frac{\partial \mathbf{X}}{\partial r}\times\frac{\partial \mathbf{X}}{\partial s}\right|+\mathbf{F}(r,s,t)\cdot\mathbf{n}=0. \tag{13}$$

Combining these equations and using the fact that $\mathbf{F}(r,s,t)$ is normal to the boundary as discussed above, we obtain

$$(\frac{\partial \mathbf{X}}{\partial t}(r,s,t)-\mathbf{U}(r,s,t)))=M\,\mathbf{F}(r,s,t)/\left|\frac{\partial \mathbf{X}}{\partial r}\times\frac{\partial \mathbf{X}}{\partial s}\right|. \tag{14}$$

Note that the tangential no-slip condition is automatically satisfied in Eq. (14), i.e.,

$$(\frac{\partial \mathbf{X}(r,s,t)}{\partial t}-\mathbf{U}(r,s,t))\cdot\boldsymbol{\tau}=0. \tag{15}$$

One can see that our IB formulation has the advantage of not needing to evaluate the pressure differences between bubbles in order to move the internal boundaries of the foam, since the relative slip between such a boundary and the fluid can be naturally found directly from the boundary force. This is important, since the pressure is only computed on the uniform grid that is used for the fluid mechanics (see next section), and the internal boundaries of the foam cut through this grid without being constrained to conform to it in any way, so the direct evaluation of the fluid pressure on the two sides of an internal boundary would require some sort of extrapolation procedure. This is completely avoided here, since our formulation makes no explicit reference to the pressure at all.

3 Numerical scheme

3.1 Computational procedure

What has been stated so far is the mathematical formulation of the problem in immersed boundary form (i.e., with delta-function forces instead of explicit boundary conditions). For the numerical implementation, we use a first-order IB method, generalized to take a permeable foam boundary into account [6]. We use a superscript to denote the time level; thus, $\mathbf{X}^n(r,s)$ is a shorthand for $\mathbf{X}(r,s,n\Delta t)$, where Δt is the duration of the time step, and similarly for all other variables.

Throughout this section, we simplify the notation by considering only one of the internal boundaries of the foam. Since there are many such internal boundaries, the numerical procedures we describe below, in particular Steps 1, 2, and 4, need to be applied to all of them. The step-by-step procedure for the time integration from time level n to time level $n+1$ can be summarized as follows.

Step 1: Using the position of the internal boundary $\mathbf{X}^n$, calculate the Lagrangian force density $\mathbf{F}^n$. To simplify the notations, we shall use $\mathbf{F}$ and $\mathbf{X}$ instead of $\mathbf{F}^n$ and $\mathbf{X}^n$, respectively. We describe the foam boundary $\mathbf{X}$ by a triangulation $\{T^k\}$ with vertices $\{\mathbf{X}_1^k, \mathbf{X}_2^k, \mathbf{X}_3^k\}$ where k is the index for triangles. Then the discretized form of the energy functional in Eq. (9) can be written as

$$E[\mathbf{X}^n] = \gamma \sum_k |T^k| = \gamma \sum_k \frac{1}{2} |(\mathbf{X}_2^k - \mathbf{X}_1^k) \times (\mathbf{X}_3^k - \mathbf{X}_1^k)|, \tag{16}$$

where $|T^k|$ is the area of the triangle T^k.

Let us denote the force density acting on the vertex $\mathbf{X}_1^k$ as $\mathbf{F}_1^k$. Then, using the formula $\mathbf{F}_1^k \, \Delta r \, \Delta s = -\nabla_{\mathbf{X}_1^k} E$, that is, the negative gradient of E with respect to the vector $\mathbf{X}_1^k$, we can derive the discrete form of the force density as

$$\begin{aligned} \mathbf{F}_1^k &= -\frac{\gamma}{\Delta r \, \Delta s} \sum_{k=1} \frac{1}{2} \frac{\partial}{\partial \mathbf{X}_1^k} |(\mathbf{X}_2^k - \mathbf{X}_1^k) \times (\mathbf{X}_3^k - \mathbf{X}_1^k)|, \\ &= \frac{\gamma}{2\Delta r \, \Delta s} (\mathbf{X}_3^k - \mathbf{X}_2^k) \times \mathbf{n}_1^k, \end{aligned} \tag{17}$$

where $\mathbf{n}_1^k = (\mathbf{X}_2^k - \mathbf{X}_1^k) \times (\mathbf{X}_3^k - \mathbf{X}_1^k)/|(\mathbf{X}_2^k - \mathbf{X}_1^k) \times (\mathbf{X}_3^k - \mathbf{X}_1^k)|$. See the Appendix for the detailed derivation. The force density $\mathbf{F}_2^k$ (or $\mathbf{F}_3^k$) acting on the vertex $\mathbf{X}_2^k$ (or $\mathbf{X}_3^k$) can be obtained by using an appropriate permutation of the ordered set $\{\mathbf{X}_1^k, \mathbf{X}_2^k, \mathbf{X}_3^k\}$ in Eqs. (16)-(17). Note that any one vertex $\mathbf{X}_i^k$ appears in several triangles, so it is necessary to sum the force densities over all of these triangles to get the total force density on $\mathbf{X}_i^k$.

Step 2: Distribute this tension force defined on Lagrangian grid points into the force at Eulerian spatial grid points to be applied in the Navier-Stokes equations. This is done by a discretization of Eq. (7) as

$$\mathbf{f}^n(\mathbf{x}) = \sum_k \sum_{i=1}^{3} \mathbf{F}_i^k \delta_h(\mathbf{x} - \mathbf{X}_i^k) \Delta r \Delta s, \tag{18}$$

where $\mathbf{x} = (x_1, x_2, x_3)$ is the fluid mesh point, and δ_h is the smooth version of Dirac delta function [10, 15].

Step 3: Given the Eulerian force density $\mathbf{f}^n(\mathbf{x})$, we are ready to solve the descritized version of the fluid equations Eqs. (4)-(5):

$$\rho(\frac{\mathbf{u}^{n+1} - \mathbf{u}^n}{\Delta t} + \frac{1}{2}\sum_{i=1}^{3}(u_i D_i^0 \mathbf{u} + D_i^0(u_i \mathbf{u}))^n) + \mathbf{D}p^{n+1} = L\mathbf{u}^{n+1} + \mathbf{f}^n, \tag{19}$$

$$\mathbf{D} \cdot \mathbf{u}^{n+1} = 0. \tag{20}$$

In (19)-(20), D_i^0 is the standard central difference operator in the spatial direction denoted by i, where $i = 1, 2, 3$, and L is the standard 7-point discrete Laplacian. Note that Eqs. (19)-(20) are a linear system with constant coefficients in the unknowns $\mathbf{u}^{n+1}$ and p^{n+1}. With the periodic boundary conditions, we solve this linear system using Fourier transform methodology.

Step 4: Update the foam boundary points which are moved at the local fluid velocity of the updated velocity field, corrected by the relative slip. This is done by approximating Eq. (7) as follows:

$$\frac{\mathbf{X}_i^{n+1} - \mathbf{X}_i^n}{\Delta t} = \sum_{\mathbf{x}} \mathbf{u}^{n+1}(\mathbf{x}) \delta_h(\mathbf{x} - \mathbf{X}_i^n) h^3 + \frac{M \sum_{j=1}^m \mathbf{F}_{i_j}^{k_j} \Delta r \Delta s}{\sum_{j=1}^m |T^{k_j}|/3}, \tag{21}$$

where the triangles T^{k_j}, $j = 1,...,m$, have a common vertex $\mathbf{X}_{i_j}^{k_j}$ which we shall denote by $\mathbf{X}_i^n$. Thus $\sum_{j=1}^m \mathbf{F}_{i_j}^{k_j}$ is the total force density acting on the boundary point $\mathbf{X}_i^n$ and, $\sum_{j=1}^m |T^{k_j}|/3$ is the one-third of the total area of the triangles which have the vertex $\mathbf{X}_i^n$ in common.

3.2 Some implementation details

(A) No permeability at the junctions : We assume that there is no permeability at the junctions where three (or more) internal boundaries meet. These junctions simply move at the local fluid velocity, that is, by Eq. (21) with $M = 0$. To allow permeability at the junction lines would result in inconsistencies, since the normal direction is not uniquely defined there. Physically, the lack of permeability at junction points is enforced by an accumulation of liquid at such points, resulting in a slight thickening and smoothing out of the junction. An interesting mathematical consequence of the assumption that there is no permeability at the junction itself is that, by continuity, the flux through an internal boundary must approach zero as a junction is approached. This can only happen if the pressure difference, and hence the curvature, approaches zero as the junctions are approached. Thus our internal boundaries are locally flat at their end points. This does not need to be imposed as a boundary condition, since deviations from such local flatness will be automatically corrected by the dynamics of the numerical scheme.

(B) The maintenance of foam boundary point resolution : Since the internal boundary points $\mathbf{X}_k^n$ of the foam move without any constraint on the distance between two adjacent points, we need to address the important issue how to maintain reasonable resolution along the boundary. If the resolution becomes too coarse, there will be leaks between the boundary points, and if it becomes too fine, there will be too severe a constraint on the time step to maintain numerical stability. We maintain proper resolution of the boundary by simply adding or deleting immersed boundary points as needed in the following way.

At each time step, we start from one end point of an internal boundary and proceed along that boundary to check the distances between neighboring boundary points $\mathbf{X}_{k+1}^n$

and $\mathbf{X}_k^n$. Whenever $|\mathbf{X}_{k+1}^n - \mathbf{X}_k^n| > h/2$, we create a new immersed boundary point halfway between them. Note that the addition of such a point does not change the length of the immersed boundary at all, and therefore it has no effect on the potential energy of the boundary. Whenever $|\mathbf{X}_{k+1}^n - \mathbf{X}_k^n| < h/4$, we delete both points and create in their place a new boundary point halfway between them. An exception to this rule is that the end points of an internal boundary are never deleted. When a neighboring point to an end point is within the lower-limit distance of the end point ($h/4$), the neighboring point is simply deleted. Unlike addition of points, deletion does slightly change the potential energy of the boundary, but only by lowering it. Thus, deletion may be viewed as a kind of numerical dissipation of energy. This loss of energy is part of the numerical error of the scheme.

(C) Implementation of no-slip boundary conditions by applying a boundary feedback force : To complete the description of the numerical IB method, we need to explain the boundary conditions imposed along the edges of our computational domain. As discussed before, we use periodic boundary conditions in both space directions for the fluid equations. Despite this, we are able to impose the no-slip condition at the edges of the computational domain by laying out an array of "target points" along those boundaries. Let $\mathbf{Z}(r, s, t)$ be the target points along the boundaries, then the method used to impose no-slip condition is to apply to the boundary by the following force:

$$\mathbf{F}_0(r, s, t) = c_0(\mathbf{Z}(r, s, t) - \mathbf{X}(r, s, t)), \tag{22}$$

where c_0 is a large constant and $\mathbf{X}(r, s, t)$ is immersed boundary points that moves at the local fluid velocity and applies $\mathbf{F}_0(r, s, t)$ locally to the fluid. This provides a feedback mechanism for computing the boundary force needed to enforce the no-slip condition. In the present paper, the target points $\mathbf{Z}(r, s, t)$ are sometimes fixed (i.e., independent of time), to simulate stationary walls, and sometimes they move along the boundaries of the domain in a prescribed manner to simulate sliding walls. Note that the target-point method for enforcing the no-slip condition still allows for the usage of FFT, since we do so not by changing the boundary conditions per se but instead by applying forces that effectively

prevent the fluid from moving, or force it to move in a prescribed manner at the specified locations.

4 Results and Discussion

4.1 Initial setting

Consider a computational domain Ω filled with an incompressible fluid in which foam boundaries are immersed and divide the fluid into several cells, see Figure 2. Throughout this paper, we fix the computational domain $\Omega = [0,1] \times [0,1] \times [0,1]$, and the no-slip (rigid) boundary conditions are imposed along the circular cylinder $(x-1/2)^2+(y-1/2)^2 = (1/2)^2$, unless otherwise stated.

For the boundaries of the foam, we choose a part of a circular cylinder with the radius 0.25 and the height 0.5, and put it at the center of the computational domain. Then n equally-spaced edges are chosen along the side of the circular cylinder and connected with n radial planes to the rigid boundary (outer cylinder). These planes also divide the circular arcs on the top and bottom of the cylinder into n edges, and we construct surfaces containing these edges and the corresponding edges of the rigid boundary. These surfaces intersect with the radial planes to make new edges as illustrated in Figure 2.

This construction procedure generates an initial foam boundary which is composed of the boundary of the inner circular cylinder, n radial planes, and the surfaces emanating from the n edges on the circular arcs of the top and bottom of the inner cylinder. Thus, the total numbers of cells, the boundaries, and the edges (triple junctions) are $n+3$, $4n+2$, and $5n$, respectively. Also the inner cell, which is the inner circular cylinder, has $n+2$ boundaries and $3n$ edges. Figure 2 shows two cases of this type of foam, $n = 4$ and $n = 8$, which also represents the triangulation of each foam boundary.

The mesh width of the computational domain, $h = \Delta x = \Delta y = 1/64$, is uniform and fixed in time, and the time step duration is $\Delta t = 10^{-4}$. The fluid density is chosen as $\rho = 1$, the viscosity $\mu = 0.01$, and the surface tension γ used in Eq. (9) is fixed at 1.0. We use

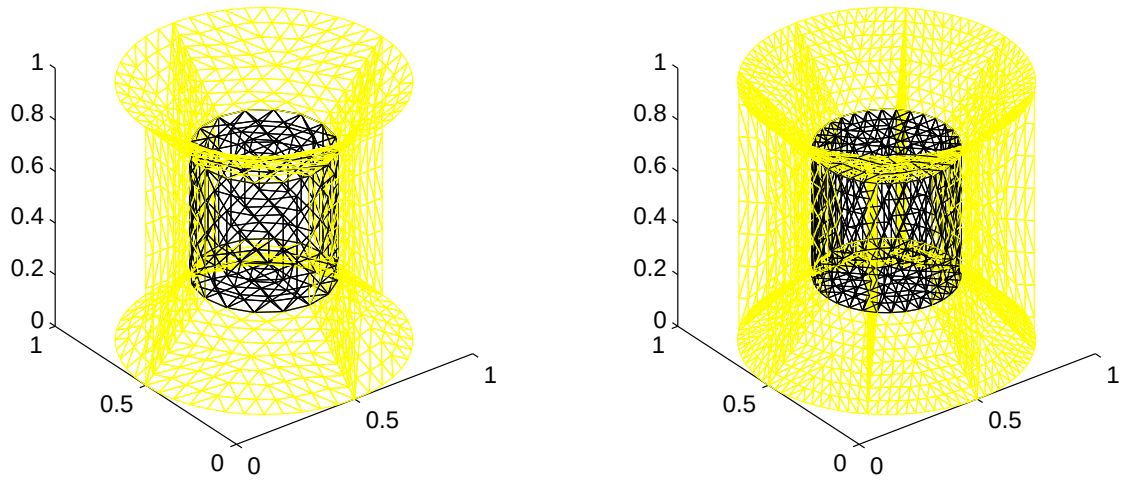

Figure 2: Foam boundary as a combination of the boundary of an inner circular cylinder, n radial planes, and surfaces emanating from the n edges on the circular arcs of the top and bottom of the inner cylinder. The left has $n = 4$, and the right has $n = 8$. The surfaces represent the foam boundaries and are triangulated initially.

two different permeabilities, M=0 and 0.01, to see how the permeability affects the foam dynamics.

4.2 Convergence study

In order to provide verification that the present IB method correctly solves the foam dynamics, we perform a convergence study. We consider a foam with a single inner cell which was constructed above with $n = 4$, see the left panel of Figure 2. We choose two different permeabilities: M=0 and 0.01. Figure 3 shows the motion of the inner cells at some selected times. Independent of the permeability, the inner cell initially changes its shape to have spherical surfaces. However, when the permeability is $M = 0$, the inner cell does not change its volume before and after it reaches the shape of the spherical surfaces as its steady. When the permeability is 0.01, the inner foam changes its shape and also reduce its volume.

Now we choose the mesh sizes of the domain N=32, 64, and 128 so that the correspond-

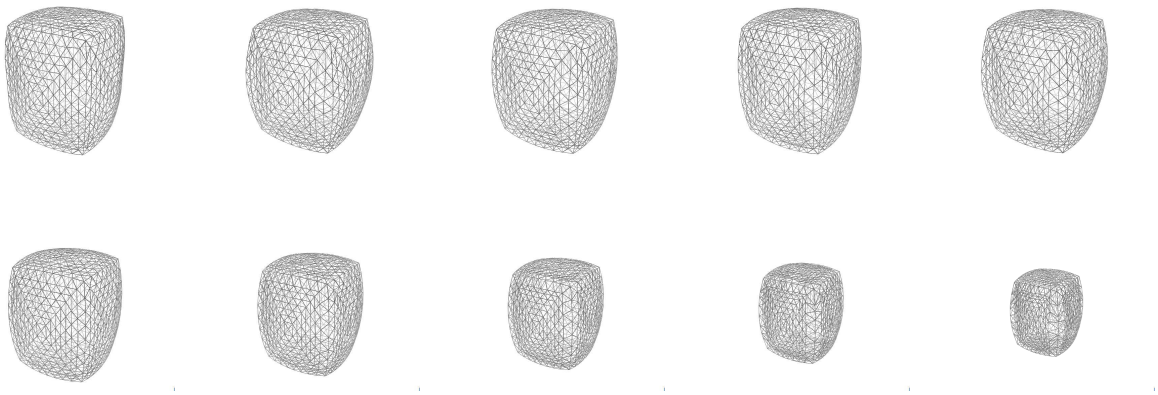

Figure 3: Motion of the inner cells. The permeability is $M = 0$ on the top and $M = 0.01$ on the bottom. The times are 0.2, 0.4, 0.6, 0.8, and 1.0 on the top, and 0.8, 1.6, 2.4, 3.2, and 4.0 on the bottom. The inner cells in both cases initially change their shape to reach the spherical surfaces, after which, while the inner foam with the permeability $M = 0$ keeps its shape (top), the inner cell with a positive permeability decreases.

ing mesh width is $h = 1/N$. We also choose Δt proportional to h, so that each factor of two in refinement of the fluid mesh width is accompanied by the same factor of refinement for the boundary mesh and the time step duration.

The left of Figure 4 shows the volume of the inner cell as a function of time for the three N's and the two permeabilities. We can see that, while the volume of the inner foam with the permeability $M = 0$ is a constant in time, that with a positive permeability decreases. We can also observe that, for each permeability, the volume changes are close for the three cases of N's. Especially, The difference of the volumes between the cases of $N = 64$ and 128 is smaller than that between the cases of $N = 32$ and 64, which might imply the convergence behavior of the solutions.

To get a more quantitative measure of convergence, we compare the velocity fields computed on the three different meshwidths. Figure 4 shows the convergence ratios of the computed fluid velocity $\mathbf{u}(\mathbf{x}, t)$. Since we do not know the exact solution of the problem, the estimation of the convergence ratio requires three numerical solutions for three consecutive N's. Let (u_N, v_N, w_N) be the velocity field, and let $||\cdot||_2$ be L_2 norm. The left panel of Figure

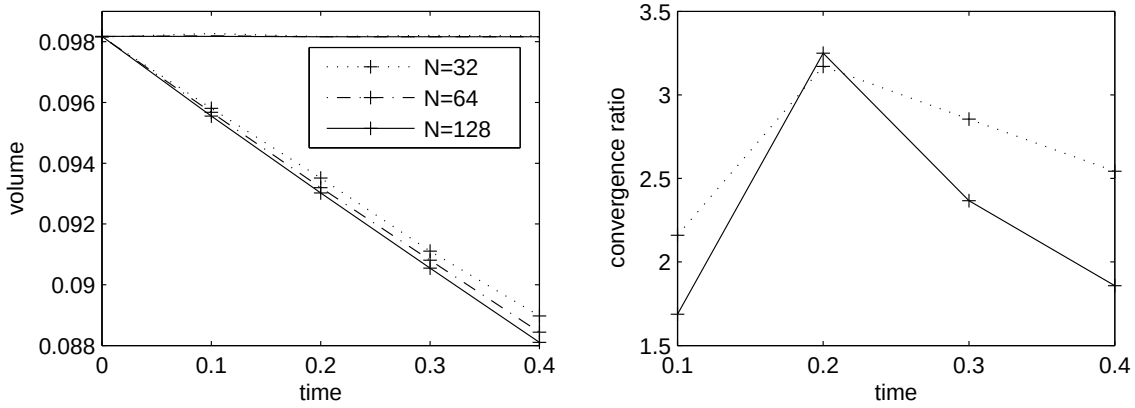

Figure 4: The volume changes of the inner cell in terms of time for the three N's and the two permeabilities (left) and the convergence ratios of the computed velocity field $\mathbf{u}(\mathbf{x}, t)$ of the fluid (right). The dotted line is the convergence ratio for $M = 0$, and the solid line is the rate for $M = 0.01$. The convergence ratios are near 2 (first order accuracy).

4 shows the convergence ratios $(||u_N - u_{2N}||_2^2 + ||v_N - v_{2N}||_2^2 + ||w_N - w_{2N}||_2^2)^{1/2}/(||u_{2N} - u_{4N}||_2^2 + ||v_{2N} - v_{4N}||_2^2||w_{2N} - w_{4N}||_2^2)^{1/2}$ versus time for $N = 32$. One can see from the figure that the convergence ratios for the fluid velocity are around two, which indicates that the present method is first-order accurate.

4.3 Foam with a single inner cell

The derivation of 3D generalized von Neumann relation in Eq. (2) can be based on the following formula:

$$\int_{\partial \mathbf{D}} H \, dS = -2\pi(\mathcal{L}(\mathbf{D}) - \frac{1}{6}\sum_{i=1}^{n} e_i(\mathbf{D})). \tag{23}$$

for a domain $\mathbf{D}$ with mean width $\mathcal{L}(D)$ bounded by a surface $\partial\mathbf{D}$ consisting of smooth surfaces that meet along curves (edges) $e_i(\mathbf{D})$ with dihedral exterior angle $pi/3$ measured in the plane perpendicular to $e_i(\mathbf{D})$. Here dS is an element of area on $\partial\mathbf{D}$, and H is the sum of the principle curvatures.

Although the definition of the mean width in terms of Euler characteristics [5] is useful

for proving the formula, it is not easy to use to compute the mean width of an arbitrary domain $\mathbf{D}$. However, there are some other ways of calculating the mean width analytically for certain special shapes, and also numerically for arbitrary domain. First, if the domain $\mathbf{D}$ is a polyhedron with flat faces and μ edges, we have

$$\mathcal{L}(\mathbf{D}) = \frac{1}{2\pi} \sum_{i=1}^{\mu} L_i \theta_i, \tag{24}$$

where L_i is the length of edge i and θ_i is the exterior (turning) angle at edge i. The formula (24) can be proven using some properties of the mean width [5] or using the direct computation of the mean curvature of the polyhedron $\mathbf{D}$ where the mean curvature H is localized only in the edges [4]. For example, if $\mathbf{D}$ is a cube with length $L_i = a$, since $\theta_i = \pi/2$, $\mathcal{L}(\mathbf{D}) = 3a$. Note that the exterior angles θ_i are not what is required for a domain $\mathbf{D}$ of a foam which is $\pi/3$.

We can approximate the mean width of an arbitrary domain in three dimensions using a triangulation of the domain, which we have used to describe the foam boundaries in our simulations. Since the triangles meet other triangles with a common edge, we can consider the domain $\mathbf{D}$ as a polyhedron with triangular faces, and its mean width can be computed by the formula (24). Note that the turning angles θ_i may be positive or negative depending on whether the surface curvature in the direction perpendicular to the edge is convex or concave, respectively. Note that the mean width of an arbitrary domain $\mathbf{D}$ can be approximated by that of the triangulation of the domain $\mathbf{D}$ which can be computed numerically.

Among the edges of all the triangular faces of the domain $\mathbf{D}$, we denote the index $i \in E$ for the edges which constitute the triple junction of the foam. Now with the triangulated domain $\mathbf{D}$ and the above formula (24), the 3D von Neumann relation (2) can be written as

$$\begin{aligned} \frac{dV}{dt} &= -M\,\gamma\,(\sum_{i=1}^{\mu} L_i\theta_i - \frac{\pi}{3}\sum_{i\in E} L_i), \\ &= -M\,\gamma\,(\sum_{i=1}^{\mu} L_i\theta_i - \sum_{i\in E} L_i\theta_i). \end{aligned} \tag{25}$$

In the first equation, we use the assumption that the dihedral exterior angles are all $\pi/3$

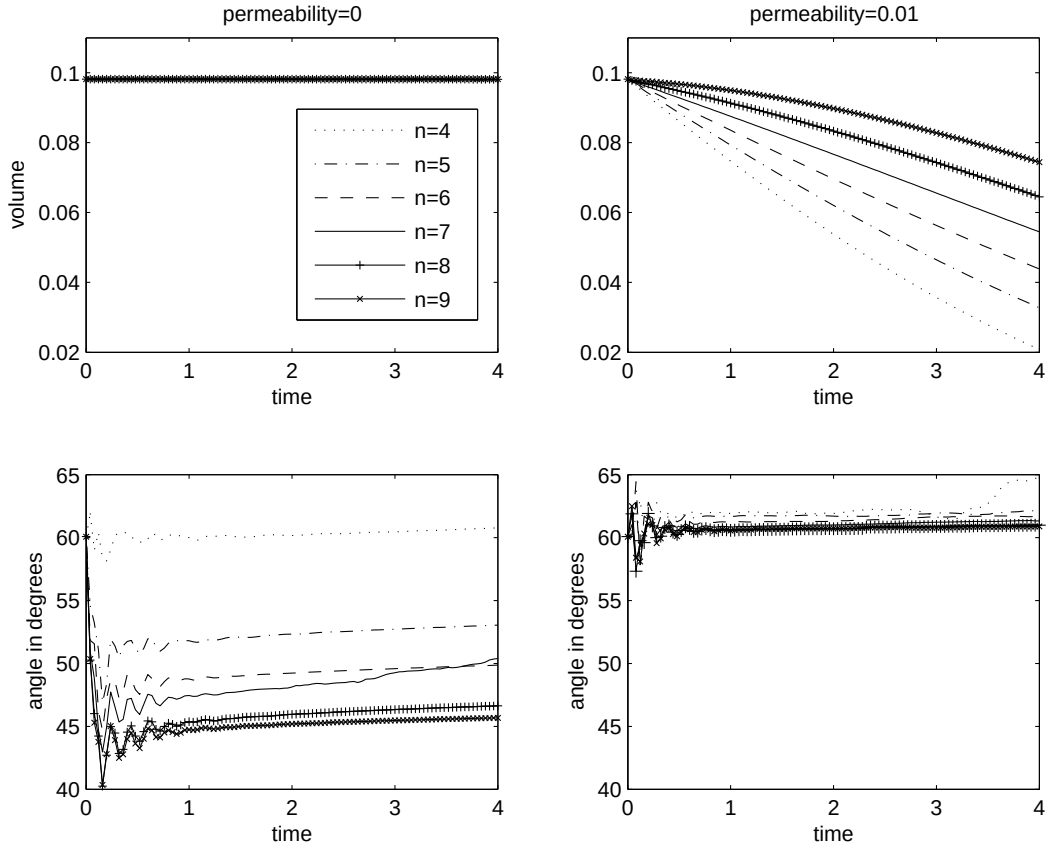

Figure 5: The volume of the inner cell (top panels) and the average angle at the triple junctions (bottom panels) as functions of time for the two permeability parameters: $M = 0$ (left panels) and $M = 0.01$ (right panels).

between two triangles along the triple junction of the foam. In the second equation, however, these angles are computed directly from the two triangles along the triple junction. The difference between these two angles can be seen as a numerical error.

In order to check the 3D von Neumann relation (25), we consider two different permeability parameters $M = 0$ and $M = 0.01$, and several different inner foams with the radial plane from $n = 4$ to $n = 9$. Figure 5 plot the volume of the inner cell (top panels) and the average angle at the triple junctions (bottom panels) as functions of time for the two permeability parameters: $M = 0$ (left panels) and $M = 0.01$ (right panels). When there is no permeability ($M = 0$), the volume of the inner cell does not change. When the per-

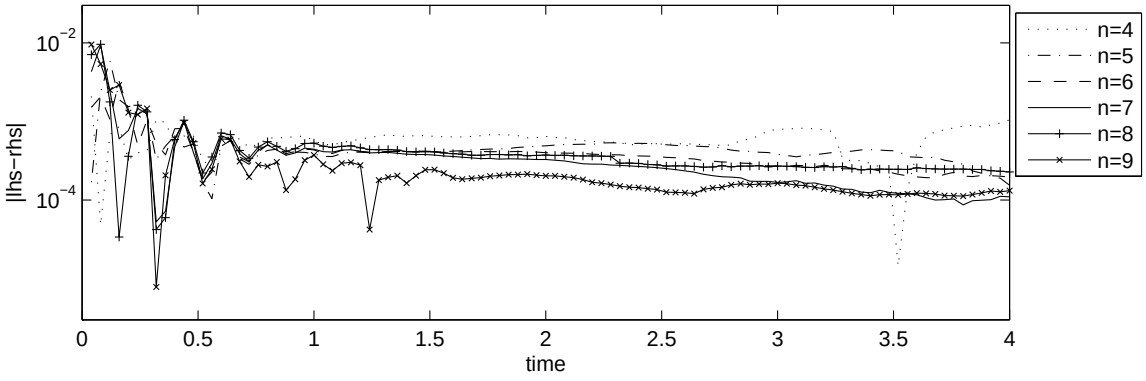

Figure 6: Graphs of $|lhs - rhs|$ in terms of time as logarithmic scale where lhs and rhs are defined in the text. The right and left hand sides of (26) are close, which confirms the 3D generalized von Neumann relation (25) and thus (2) qualitatively.

meability is nonzero, the volumes of the inner cells decrease. From the left panels, we can see that the dihedral angle averaged over the triple junctions is around $\pi/3$ (60 in degrees), which implied that the assumption that the boundaries of the domain $\mathbf{D}$ meet along triple edges with dihedral exterior angle $\pi/3$ is correctly imposed in the theory.

Unlike the 2D von Neumann relation, the 3D von Neumann relation is not topological. The rate of change of the volume of a given domain (a curved polyhedron) in a three-dimensional dry foam is dependent on the domain size as well as the number of faces of the cell. Thus the volume change is not linear, and we have to check the discrete von Neumann relation (25) at each time iteration. To do that, we record the volume of the inner cell $V(t)$, the length $L_i(t)$ of the edge i, and the exterior (turning) angle $\theta_i(t)$ at edge i at time level t. Then the trapezoidal rule for (25) (first equation) gives the following discretized equation:

$$\begin{aligned}\frac{V(t+\Delta t) - V(t)}{\Delta t} = &- M\,\gamma\,(\sum_{i=1}^{\mu}(L_i(t+\Delta t)\,\theta_i(t+\Delta t) + L_i(t)\,\theta_i(t))/\,2 \\ &- \sum_{i\in E}(L_i(t+\Delta t)\,\theta_i(t+\Delta t) + L_i(t)\,\theta_i(t))/\,2\,). \end{aligned} \tag{26}$$

Let the right and left hand sides of (26) be lhs and rhs, respectively, Figure 6 draws $|lhs - rhs|$ in terms of time as logarithmic scale. The inner foam has the radial plane from $n = 4$ to $n = 9$, and the permeability parameter is $M = 0.01$. We can see from the figure

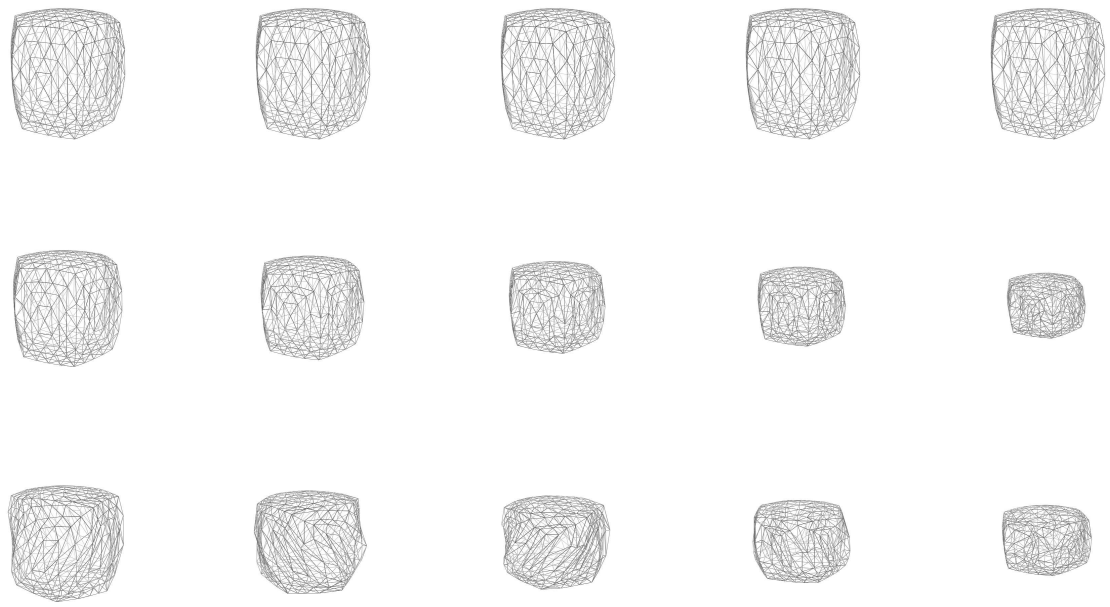

Figure 7: Motions of the inner foam which has the radial plane $n = 6$ with three different cases: zero permeability in a steady flow (top), permeability $M = 0.01$ in a steady flow (middle), and permeability $M = 0.01$ in a dynamic flow (bottom) The times are 1, 2, 3, 4, 5, and 6.

that the right and left hand sides of (26) are close, which confirms the 3D generalized von Neumann relation (25) and thus (2) qualitatively.

We can see from Figure 5 that the volumes of the inner cell with the radial plane from $n = 4$ to $n = 9$ all decrease in time. However, it is known that, when a cell has a number of faces larger than some critical number, the volume increases. The critical number of faces which have been found theoretically or experimentally is between 14 and 16. In order to find the critical number numerically, we simulate the 3D foam which has the inner cell with the radial plane from $n = 10$ to $n = 16$. Note that the inner cell with n radial plane has $n + 2$ faces. Figure 5 plot the volume of the inner cell (top panels) and the average angle at the triple junctions (bottom panels) as functions of time for the two permeability parameters: $M = 0$ (left panels) and $M = 0.01$ (right panels).

The fluid dynamics of a foam is not necessarily restricted to the slow coarsening regime

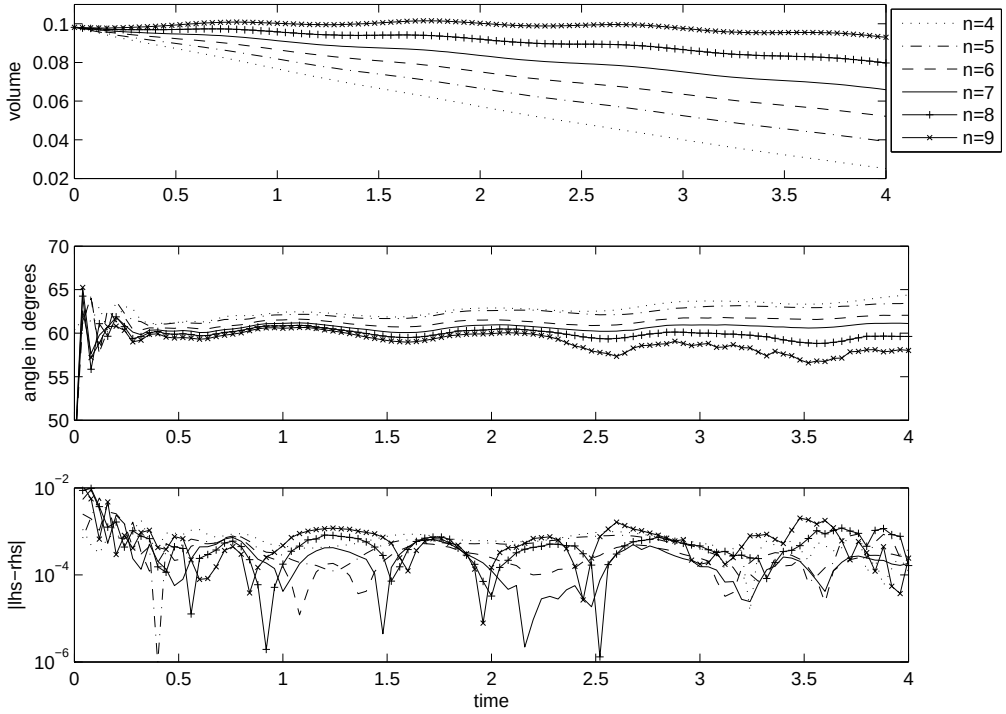

Figure 8: The volume of the inner cell (top panel), the average angle at the triple junctions (middle panel), and $|lhs - rhs|$ (logarithmic scale) as functions of time.

that has been considered up to now. To illustrate this, we use the same initial configuration of the foam as in Figure 2 in which we have used no-slip (rigid) wall along the circular cylinder represented as $(\frac{1}{2} + \frac{1}{2}\cos\theta, \frac{1}{2} + \frac{1}{2}\sin\theta, z)$, where $0 \leq \theta \leq 2\pi$ and $0 \leq z \leq 1$. Instead of using the fixed wall, we create target points which rotate on the rigid wall in an oscillatory manner. This motion of the target points can be created by defining the surface as

$$(\frac{1}{2} + \frac{1}{2}\cos(\theta + \theta(z,t)), \frac{1}{2} + \frac{1}{2}\sin(\theta + \theta(z,t)), z), \tag{27}$$

where $\theta(z,t) = A\sin(2\pi z)\sin(2\pi\omega t)$, $0 \leq \theta \leq 2\pi$, and $0 \leq z \leq 1$. The target points on the cylinder rotates right and left with amplitude $A\sin(2\pi z)$ and frequency ω. We here use $A = \pi/4$ and frequency is $\omega = 0.5$.

Figure 7 shows the motions of the inner foam which has the radial plane $n = 6$ with three different cases: zero permeability in a steady flow (top), permeability $M = 0.01$ in a steady flow (middle), and permeability $M = 0.01$ in a dynamic flow (bottom). We can

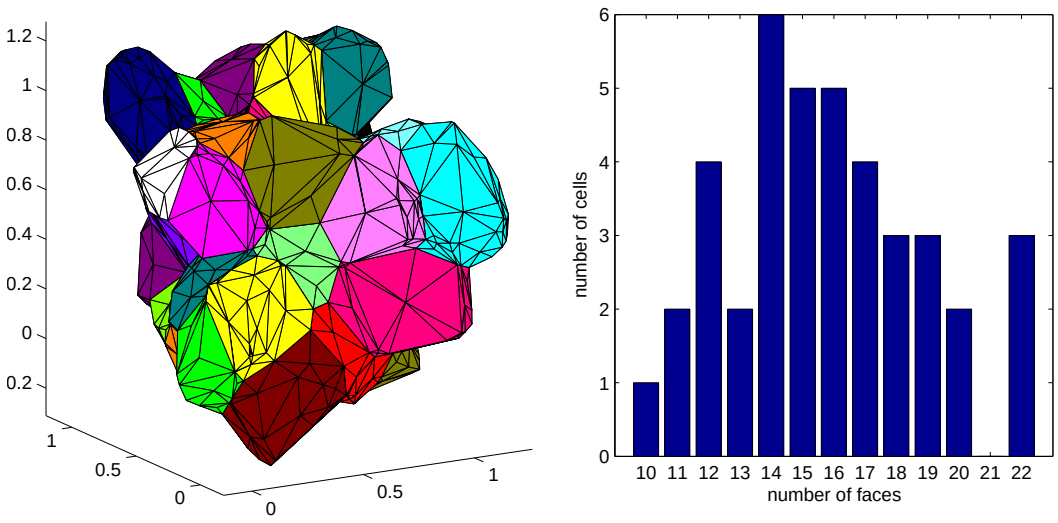

Figure 9: The initial configuration of a general foam (left) and the numbers of cells versus the numbers of faces (right).

clearly observe the interaction between the foam boundaries and the fluid flow (bottom). Even though the foam is now far from equilibrium, the areas of the inner cells still follow closely the von Neumann relation, see the lower panel of Figure 8.

4.4 General Foams

We now consider more general foam configurations. While we use the same computation domain $\Omega = [0,1] \times [0,1] \times [0,1]$ as before, here we use the periodic boundary conditions without the rigid wall. We construct a Voronoi diagram to set up an initial configuration of a foam [**?**]. To do that, we first choose randomly a set of points in Ω which will sit inside each cell of a foam. In order to take the periodicity into account, we extend the unit cube into a cube $[-1,2] \times [-1,2] \times [-12]$ and copy the set of points chosen in Ω periodically into the extended cube. Next, we construct the Delauney tessellation which divides the space into a set of regions of which apices belong to the set of the initially chosen points. Now we consider only the unit cube Ω as the computational domain in which a network of foam boundaries exist periodically, see Figure 9 which shows the initial configuration of a general

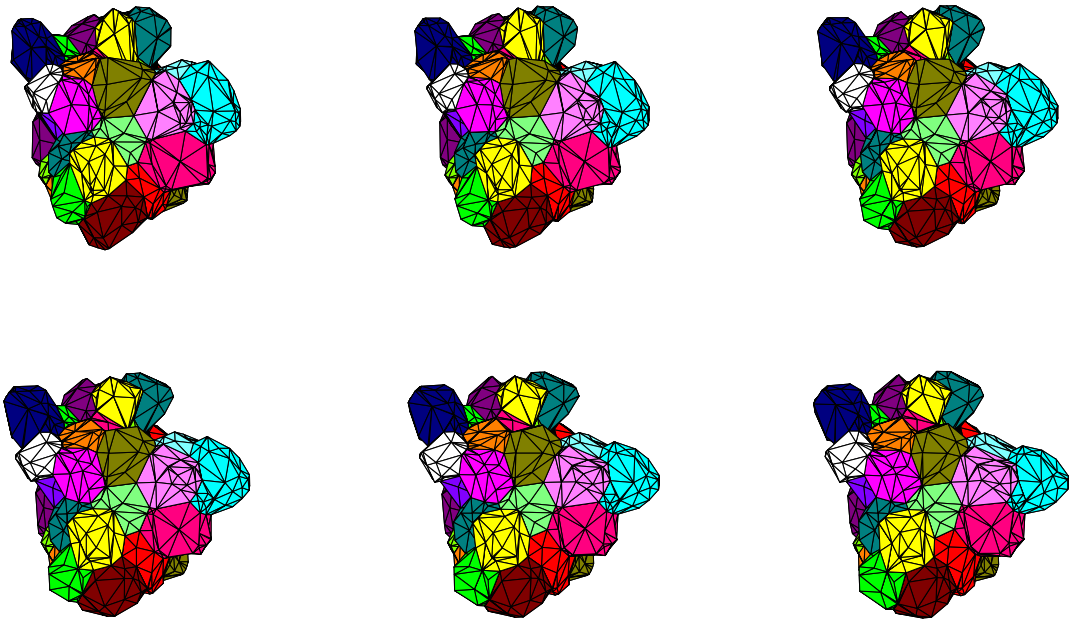

Figure 10: The motion of a general foam at some chosen times: 0.12, 0.24, and 0.36 (top), and 0.48, 0.6, and 0.72 (bottom).

foam. The left panel describes how many cells have the given number of faces. For example, only one cell of the foam has 10 faces, 6 cells have 15 faces, and 3 cells have 22 faces.

Figure 10 shows the motion of the general foam at some chosen tiems: 0.12, 0.24, and 0.36 (top), and 0.48, 0.6, and 0.72 (bottom). Since the initial foam is composed of planar faces, we can observe clear motions of some cells, compare the 1st and last ones. After some transient time, the foam does not show clear movement, especially it is difficult to differ the last two configurations. Even though the foam seems to stop moving, the foam continues to change. In order to see that, we carefully look at the motions of two cells in time and volume changes of some selected cells, see Figure 11.

The top panel of Figure 11 shows the motion of two cells with 12 faces (small one) and 22 faces (larger one) at some chosen times: 0, 3, and 6. We can observe that, while both

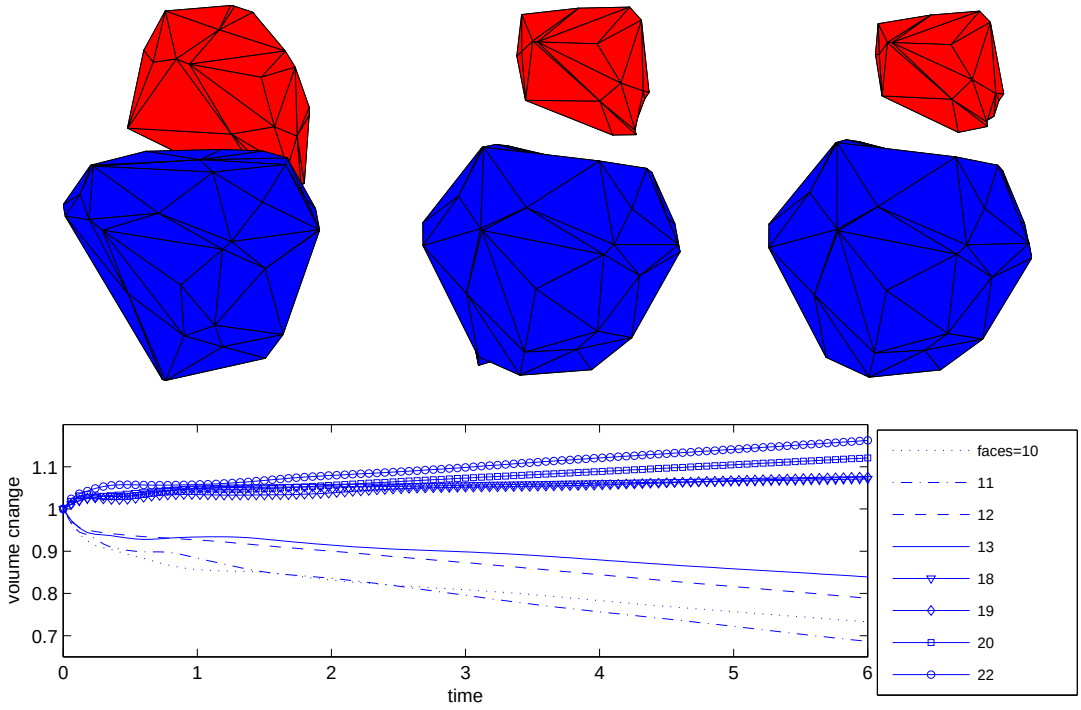

Figure 11: The motion of two cells with 12 faces (small one) and 22 faces (larger one) at some chosen times: 0, 3, and 6 (top) and the volume change in terms of time for some selected cells (bottom).

cells change their shape, the cell with 12 faces decreases its volume and the cell with 22 faces increases its volume. The bottom panel draws the volume change in terms of time for some selected cells. The volume is averaged over the cells with the same number of faces, for example, the volume of the 22-faced cells is the average volume of all the 22 faced cells. We see that there are 3 cells have 22 faces from Figure 9. Whereas the volumes of the cell with small number of faces decrease, the volumes of the cells with large number of faces increase. Even though the cell volumes are not linear in time as suggested in the 2D von Neumann relation, the overall volume changes induce the coarsening of a foam structure. More detailed investigation on the coarsening is left as a subject for future work.

5 Summary and Conclusions

We have presented an immersed boundary method to simulate the fluid dynamics of a two-dimensional dry foam. We model the gas phase of the foam as a viscous incompressible fluid, and the liquid phase as a massless network of permeable internal boundaries under surface tension. The internal boundary force, generated by the surface tension, is everywhere normal to the internal boundaries. Permeability is modeled by allowing the internal boundaries to slip relative the fluid, at a velocity (speed *and* direction) proportional to the boundary force. This is equivalent to slip in the normal direction only at a speed proportional to the pressure difference across each internal boundary, and thus models correctly the diffusion of gas through the liquid phase of the foam.

An algorithm is described that maintains the resolution of each internal boundary within predetermined bounds despite arbitrarily large changes in length of the internal boundary.

We have validated the method by checking that the von Neumann relation is well satisfied, except when the assumptions under which it was derived are violated. A striking fact, confirmed by our results, is that the derivation of the von Neumann relation does *not* require the assumption of uniform curvature along each internal boundary, and therefore does not require uniform pressure within each bubble of the foam. The von Neumann relation therefore remains valid in dynamical situations with nontrivial fluid dynamics in the gas phase of the foam, as we have seen. Additional validation has been provided in the form of a convergence study, which confirms the expected first-order accuracy of the scheme.

Within the context of two-dimensional foams, the principal limitation of the method as currently implemented is that we do not allow for the resolution of quadruple or higher order junctions into triple junctions. A more important limitation, of course, is the restriction to the two-dimensional case. The extension of the methodology introduced here to the study of three-dimensional foams will be the subject of future work.

6 Summary and Conclusions

Acknowledgement The second author was supported in part by the MoE-ATU project and the National Science Council of Taiwan under grant NSC95-2115-M-009-010.

Appendix. We here derive the force density using the variational derivative of an energy functional. First suppose that the energy functional is given as

$$E[\mathbf{X}] = \gamma \int |\mathbf{X}_r \times \mathbf{X}_s| \, drds, \tag{28}$$

where $X(r,s)$ is a parameterized surface and $\mathbf{X}_r = \frac{\partial \mathbf{X}}{\partial r}$ and $\mathbf{X}_s = \frac{\partial \mathbf{X}}{\partial s}$, see Eq. (9). Let $\mathbf{X} + \epsilon \mathbf{Y}$ be a perturbation of $\mathbf{X}$, then the variational derivative is defined as follows:

$$\begin{aligned}
\int \frac{\partial E}{\partial \mathbf{X}}(r,s) \cdot \mathbf{Y}(r,s) drds &= \lim_{\epsilon \to 0} \frac{E[\mathbf{X} + \epsilon \mathbf{Y}] - E[\mathbf{X}]}{\epsilon} \\
&= \lim_{\epsilon \to 0} \gamma \int \frac{|(\mathbf{X}_r + \epsilon \mathbf{Y}_r) \times (\mathbf{X}_s + \epsilon \mathbf{Y}_s)| - |\mathbf{X}_r \times \mathbf{X}_s|}{\epsilon} drds \\
&= \lim_{\epsilon \to 0} \gamma \int \frac{|(\mathbf{X}_r + \epsilon \mathbf{Y}_r) \times (\mathbf{X}_s + \epsilon \mathbf{Y}_s)|^2 - |\mathbf{X}_r \times \mathbf{X}_s|^2}{\epsilon(|(\mathbf{X}_r + \epsilon \mathbf{Y}_r) \times (\mathbf{X}_s + \epsilon \mathbf{Y}_s)| + |\mathbf{X}_r \times \mathbf{X}_s|)} drds \\
&= \lim_{\epsilon \to 0} \gamma \int \frac{2\epsilon(\mathbf{Y}_r \times \mathbf{X}_s + \mathbf{X}_r \times \mathbf{Y}_s) \cdot (\mathbf{X}_r \times \mathbf{X}_s) + O(\epsilon^2)}{\epsilon(|(\mathbf{X}_r + \epsilon \mathbf{Y}_r) \times (\mathbf{X}_s + \epsilon \mathbf{Y}_s)| + |\mathbf{X}_r \times \mathbf{X}_s|)} drds \\
&= \gamma \int \frac{(\mathbf{Y}_r \times \mathbf{X}_s + \mathbf{X}_r \times \mathbf{Y}_s) \cdot (\mathbf{X}_r \times \mathbf{X}_s)}{|\mathbf{X}_r \times \mathbf{X}_s|} drds \\
&= \gamma \int (\mathbf{Y}_r \times \mathbf{X}_s + \mathbf{X}_r \times \mathbf{Y}_s) \cdot \mathbf{n} drds \\
&= \gamma \int ((\mathbf{X}_s \times \mathbf{n}) \cdot \mathbf{Y}_r + (\mathbf{n} \times \mathbf{X}_r) \cdot \mathbf{Y}_s) drds \\
&= -\gamma \int ((\mathbf{X}_s \times \mathbf{n})_r + (\mathbf{n} \times \mathbf{X}_r)_s) \cdot \mathbf{Y} drds.
\end{aligned}$$

Here $\mathbf{n} = (\mathbf{X}_r \times \mathbf{X}_s)/|\mathbf{X}_r \times \mathbf{X}_s|$ and we use the integration by parts in the last equality. According to the principle of virtual work, the force density $\mathbf{F}$ is given by

$$\mathbf{F} = -\frac{\partial E}{\partial \mathbf{X}} = \gamma((\mathbf{X}_s \times \mathbf{n})_r + (\mathbf{n} \times \mathbf{X}_r)_s) = \gamma(\mathbf{X}_s \times \mathbf{n}_r + \mathbf{n}_s \times \mathbf{X}_r). \tag{29}$$

Now, from the fact that the Weingarten map (see any differential geometry textbook) is of the matrix form with its element L_i^j for $i, j = 1, 2$ using the basis $\{\mathbf{X}_r, \mathbf{X}_s\}$, it is well

known that $\mathbf{n}_r = -L_1^1\mathbf{X}_r - L_1^2\mathbf{X}_s$ and $\mathbf{n}_s = -L_2^1\mathbf{X}_r - L_2^2\mathbf{X}_s$. Thus the force density can be further simplified as

$$\begin{aligned}\mathbf{F} &= \gamma(\mathbf{X}_s \times (-L_1^1\mathbf{X}_r - L_1^2\mathbf{X}_s) + (-L_2^1\mathbf{X}_r - L_2^2\mathbf{X}_s) \times \mathbf{X}_r) \\ &= \gamma(L_1^1 + L_2^2)\mathbf{X}_r \times \mathbf{X}_s \\ &= 2\gamma H|\mathbf{X}_r \times \mathbf{X}_s|\mathbf{n}, \end{aligned} \tag{30}$$

where H is the mean curvature. An important consequence of this derivation is that the boundary force density $\mathbf{F}$ is normal to the boundary, as we used in Section 2.

Now we consider the discretized form of force density which is also derived from the partial derivatives of the corresponding energy functional:

$$E[\mathbf{X}] = \gamma \sum_k |T^k| = \gamma \sum_k \frac{1}{2}|(\mathbf{X}_2^k - \mathbf{X}_1^k) \times (\mathbf{X}_3^k - \mathbf{X}_1^k)|, \tag{31}$$

where T^k is the triangular element with vertices $\{\mathbf{X}_1^k, \mathbf{X}_2^k, \mathbf{X}_3^k\}$. As we mentioned before, the total force on $\mathbf{X}_i^k$ is the summation of the force over all the triangles which have the vertex $\mathbf{X}_i^k$ in common. Thus it is sufficient to know how to compute force density generated from the energy functional of one triangle:

$$E[\mathbf{T}^k] = \gamma|T^k| = \gamma\frac{1}{2}|(\mathbf{X}_2^k - \mathbf{X}_1^k) \times (\mathbf{X}_3^k - \mathbf{X}_1^k)|. \tag{32}$$

Let $\mathbf{X}_1^k = X_{1,1}^k\mathbf{e}_1 + X_{1,2}^k\mathbf{e}_2 + X_{1,3}^k\mathbf{e}_3$ where $\{\mathbf{e}_1, \mathbf{e}_2, \mathbf{e}_3\}$ is the standard basis for 3D Euclidian space, then the partial derivative of the energy $E[\mathbf{T}^k]$ with respect of $\mathbf{X}_{1,i}^k$ can be computed as follows:

$$\begin{aligned}\frac{\partial E[\mathbf{T}^k]}{\partial X_{1,i}^k} &= \frac{\gamma}{2}\lim_{\epsilon\to 0}\frac{|(\mathbf{X}_2^k - \mathbf{X}_1^k - \epsilon\mathbf{e}_i) \times (\mathbf{X}_3^k - \mathbf{X}_1^k - \epsilon\mathbf{e}_i)| - |(\mathbf{X}_2^k - \mathbf{X}_1^k) \times (\mathbf{X}_3^k - \mathbf{X}_1^k)|}{\epsilon} \\ &= -\frac{\gamma}{2}((\mathbf{X}_2^k - \mathbf{X}_3^k) \times \mathbf{e}_i) \cdot \mathbf{n}_1^k, \end{aligned} \tag{33}$$

where $\mathbf{n}_1^k = (\mathbf{X}_2^k - \mathbf{X}_1^k) \times (\mathbf{X}_3^k - \mathbf{X}_1^k)/|(\mathbf{X}_2^k - \mathbf{X}_1^k) \times (\mathbf{X}_3^k - \mathbf{X}_1^k)|$. When we write the force density acting on $\mathbf{X}_1^k$ as $\mathbf{F}_1^k = (F_{1,1}^k, F_{1,2}^k, F_{1,3}^k)$, we have

$$F_{1,i}^k \Delta r \Delta s = -\frac{\partial E[\mathbf{T}^k]}{\partial X_{1,i}^k} = \frac{\gamma}{2}((\mathbf{X}_2^k - \mathbf{X}_3^k) \times \mathbf{e}_i) \cdot \mathbf{n}_1^k. \tag{34}$$

for i=1, 2, 3, and we can obtain

$$F_1^k \Delta r \Delta s = \frac{\gamma}{2}(\mathbf{X}_3^k - \mathbf{X}_2^k) \times \mathbf{n}_1^k. \tag{35}$$

This equation is used in Eq. (17) of Section 3 for the force generator. Note again that the force density $\mathbf{F}_2^k$ (or $\mathbf{F}_3^k$) acting on the vertex $\mathbf{X}_2^k$ (or $\mathbf{X}_3^k$) can be obtained by using an appropriate permutation of the ordered set $\{\mathbf{X}_1^k, \mathbf{X}_2^k, \mathbf{X}_3^k\}$.

References

[1] D. Weaire and S. Hutzler, *The Physics of Foams*, Oxford University Press, 1999.

[2] von Neumann, J. in Metal Interfaces (ed. C.Herring) 108-110(American Society for Metals, Cleveland, 1951).

[3] W.W.Mullins, *in Metal Surfaces: Structure, Energetics, and Kinetics.* (eds. W.D.Robertson and N.A.Gjostein) 17-66(American Society for Metals, Metals Park, Ohio, 1963).

[4] S. Hilgenfeldt, A. M. Kraynik, S. A. Koehler, and H. A. Stone, *An accurate von Neumann's law for three-dimensional foams*, Phys. Rev. Lett. 86(12):2685-2688, 2001.

[5] R.D.MacPherson and D.J.Srolovitz, *The von Neumann relation generalized to coarsening of three-dimensional microstructures,* Nature, 446(26):1053-1055, 2007.

[6] Y. Kim, M.-C. Lai, and C.S. Peskin, *Numerical simulations of two-dimensional foam by the immersed boundary method.* J. Comput. Phys. 229:5194-5207, 2010.

[7] Y.Kim and C.S.Peskin. *2-D parachute simulation by the Immersed Boundary Method.* SIAM J.Sci.Comput. 28(6), 2006.

[8] L. Santalo and K. Mac, *Integral Geometry and Geometric Probability,* Cambridge Univ. Press, 2004.

[9] T. Herdtle and H. Aref, *Numerical experiments on two-dimensional foam*, J. Fluid Mech. 241, 233-260, 1992.

[10] C.S.Peskin, *The Immersed Boundary Method.* Acta Numerica, 11:479-517, 2002

[11] C.S.Peskin, *Numerical analysis of blood flow in the heart.* J. Comput. Phys. 25:220-252, 1977.

[12] D.A.Nield and A.Bejan. *Convection in Porous Media.* Springer-Verlag, 1991

[13] C.S.Peskin and B.F.Printz. *Improved volume conservation in the computation of flows with immersed elastic boundaries.* J.Comput. Phys. 105:33-46, 1993

[14] M.C. Lai and Z. Li, *A remark on jump conditions for three-dimensional Navier-Stokes equations involving an immersed moving membrane*, Appl. Math. Lett., 14: 149-154, 2001.

[15] C.S.Peskin and D.M.McQueen. *Fluid dynamics of the heart and its valves. In: Case studies in Mathematical Modeling: Ecology, Physiology, and Cell Biology.* Prentice Hall, Englewood Cliffs NJ, 1996, pp. 309-337

[16] M.-C.Lai and C.S.Peskin, *An Immersed Boundary Method with Formal Second-Order Accuracy and Reduced Numerical Viscosity,* J. Comput. Phys. 160:705-719, 2000.

[17] C.S.Peskin and B.F.Printz. *Improved volume conservation in the computation of flows with immersed elastic boundaries.* J.Comput. Phys. 105:33-46,1993

[18] B.E.Griffith and C.S.Peskin, *On the order of accuracy of the immersed boundary method: Higher order convergence rates for sufficiently smooth problems.* J. Comput. Phys. 208:75-105, 2005.

[19] B.E.Griffith, X.Luo, D.M.McQueen, and C.S.Peskin, *Simulating the fluid dynamics of natural and prosthetic heart valves using the immersed boundary method.* Int. J. Appl. Mech. 1:137-177, 2009.